Coercivity Enhancement of Sintered Nd-Pr-Fe-B Magnets by Cost-Effective Grain Boundary Diffusion of Dy/Tb Films

Xin-De Zhu [1], Mei Wang [1,*], Yong-Jiang Yu [2], Qian Wang [1], Fei Wang [1], Peng-Fei Wang [2], Bin Jia [3], Cong Wang [2] and Bin Zhou [2]

[1] Key Laboratory for Liquid-Solid Structural Evolution and Processing of Materials (Ministry of Education), Shandong University, Jinan 250061, China; zhuxinde@sdu.edu.cn (X.-D.Z.)

[2] YanTai ZhengHai Magnetic Material Co., Ltd., Yantai 264006, China; yuyongjiang@zhmag.com (Y.-J.Y.); pengfei.wang@sdu.edu.cn (P.-F.W.); cong.wang@sdu.edu.cn (C.W.)

[3] State Key Laboratory of Explosion Science and Technology, Beijing Institute of Technology, Beijing 100081, China; bin.jia@bit.edu.cn

* Correspondence: wangmei@sdu.edu.cn

Abstract: High-performance sintered Nd-Pr-Fe-B magnets were successfully prepared by depositing Dy/Tb films on the surface using magnetron sputtering, which resulted in superior grain boundary diffusion (GBD) under heat treatments. The course of the diffusion was assessed using an electron probe microanalyzer (EPMA) and inductively coupled plasma (ICP). The magnetic properties and thermal stability of the magnets before and after diffusion were investigated. The results show that, mainly due to the increased and optimized Nd-Pr-rich phases and the formation of the $(Nd,Pr,Dy/Tb)_2Fe_{14}B$ shell structure surrounding the $(Nd,Pr)_2Fe_{14}B$ grains, the coercivity of the Dy- and Tb-diffused magnets was enhanced from 16.7 kOe to 24.8 kOe and 28.4 kOe, respectively, while the corresponding maximum energy product (BHmax) was 48.1 MGOe and 48.5 MGOe, respectively. The consumption of Dy/Tb in this work (0.35 wt% Dy in the Dy-diffused magnet and 0.42 wt% Tb in the Tb-diffused magnet) is much lower than that of previously reported magnets with comparable coercivity. Furthermore, Dy- or Tb-diffused magnets exhibit better thermal stability than that of the original magnet, owing to the better resistance to thermal disturbances of the magnets with optimized microstructure. This work can provide useful guidance for preparing Nd-Fe-B magnets with low cost and high performance.

Keywords: coercivity; sintered Nd-Pr-Fe-B magnet; grain boundary diffusion (GBD); magnetron sputtering

1. Introduction

Due to their excellent magnetic properties, sintered Nd-Fe-B permanent magnets have been widely used in wind power generation, information storage, medical machinery, and electric vehicles [1–3]. However, simple sintered Nd-Fe-B magnets do not meet the needs of other emerging fields. The coercivity of Nd-Fe-B magnets exhibits rapid reduction with increasing temperature, which is mainly attributed to the harmful effect of the thermal movement of atoms on the perfection of the tetragonal structure in the hard magnetic grains [4]. Thus, there is a demand for higher room-temperature coercivity to ensure the normal use of Nd-Fe-B magnets at high temperatures.

Heavy rare earth elements (HREE), such as Dy and Tb, can effectively improve the coercivity of magnets due to the formation of the $(Dy/Tb)_2Fe_{14}B$ phase with a higher magnetic anisotropy than $Nd_2Fe_{14}B$ [5–7]. However, for the conventional method of doping, in which HREE such as Dy or Tb metals are added to mother alloys, the substitution of Dy or Tb generally reduces the saturation magnetization of the 2:14:1 phase due to the antiferromagnetic coupling between Dy/Tb and Fe [8–10]. Moreover, the conventional addition of HREE increases the material cost because of the scarcity of HREE resources.

To increase coercivity with a minimum amount of HREE and a minimum reduction in remanence, grain boundary diffusion (GBD) technology was introduced into the post-processing of sintered Nd-Fe-B magnets, in which HREE sources are used to coat the magnet, and ideal effects were obtained [11,12]. During the course of the diffusion, the HREE first diffuses along the grain boundary (GB) phase, then substitutes the Nd in the $Nd_2Fe_{14}B$ lattice. As a result, a core-shell structure is obtained as the HREE diffused into the $Nd_2Fe_{14}B$ forms a $(Nd,HREE)_2Fe_{14}B$ shell, which magnetically hardens the whole magnet [13,14]. Consequently, the coercivity of the magnet is greatly improved without or with only a slight decrease in remanence, while reducing the use of HREE.

Various diffusion methods with different diffusion resources have been developed so far, such as dip coating with HREE in the form of oxides and fluorides or hydrides [11,15–17], sputtering deposition [18–20] or evaporation deposition [21–24] of pure HREE metals, and electrodeposition of fluorides [25–28]. The dip coating method involves a simple process, however, the amount of source coating cannot be precisely controlled. The electrodeposition method has a distinct advantage in fabricating smooth and thick coatings, and the thickness of the coating can be controlled by regulating the deposition potential and time. However, environmental concerns persist and the pollution problems require urgent resolution. The high vaporization points of HREE metals for GBD indicate the high costs of both the equipment and the energy consumption of evaporation deposition. Sputtering deposition can obtain stable product quality, and the thickness of coatings can be precisely controlled at a nanometer level by modifying the sputtering power and deposition time. Therefore, sputtering deposition is adopted by most researchers due to its controllable film thickness, dense film surface, and environmental friendliness.

Aiming at improving the properties of and reducing the material cost of sintered Nd-Fe-B permanent magnets, here we propose an approach to GBD that can significantly increase the coercivity of sintered Nd-Pr-Fe-B magnets using less HREE. The magnetron sputtering technique was applied to coat Nd-Pr-Fe-B magnets with Dy and Tb films. The effects of Dy/Tb diffusion on the composition distribution and microstructure of the Nd-Pr-Fe-B sintered magnets were investigated, and the magnetic properties at different temperatures were tested. The mechanism between coercivity enhancement and element distribution and the microstructure of the magnets are also discussed.

2. Materials and Methods

Sintered $Nd_{22.28}Pr_{7.03}Fe_{68.06}B_{0.986}M_{0.63}Co_{1.01}$ (M=Al, Cu, Ga, Ti, wt%) magnets were fabricated by fully automatic scale casting, hydrogenation powder production, automatic molding, continuous sintering at 1050 °C, and subsequent twice tempering (at 900 °C and 500 °C for 5 h) in a mixture of N_2, Ar, and H_2 (the base pressure was $<10^{-3}$ Pa), which is called an oxygen-free process technology [29]. The obtained Dy/Tb-free Nd-Pr-Fe-B magnets shaped in cylinders (ϕ10 mm × 10 mm) along the preferred magnetization direction were selected as the original magnets. A self-developed three-dimensional magnetron sputtering apparatus was used to deposit Dy or Tb metal film (thickness: 40 μm) to the surface of the magnets at room temperature using metallic Dy and Tb (purity: >99.9%) as diffusion sources, respectively, and then GBD was conducted in a high vacuum condition at 900 °C for 10 h, followed by annealing at 520 °C for 2 h (for more details, see [30]).

The obtained magnets were cut into 7 mm × 5 mm × 5 mm pieces, and the magnetic properties were tested at 20 °C, 100 °C, and 150 °C using an NIM-10000H hysteresigraph. Microstructure observation was performed using a conventional electron probe microanalyzer (EPMA), and the distributions of rare earth elements were further determined by line analysis. The rare earth element content of the magnets before and after GBD was measured using inductively coupled plasma (ICP).

3. Results and Discussion

3.1. Magnetic Properties

The demagnetization J–H curves of the magnets before and after GBD with Dy/Tb were measured at different temperatures (20 °C, 100 °C, 150 °C). The results are shown in Figure 1 and the corresponding magnetic properties are listed in Table 1. Through comparing the J–H curves of the Dy- and Tb-diffused magnets with the original magnets measured at 20 °C (Figure 1a), it can be seen that coercivity significantly increases from 16.7 kOe to 24.8 kOe and 28.4 kOe, respectively, showing amplifications of 48.5% and 70.0%. Elsewhere, a similar deposition technique has been recently applied for HREE diffusion, and the coercivity of the magnets was obviously enhanced. For example, Chen et al. achieved a maximum coercivity value of 14.9 kOe by Dy deposition, corresponding to an amplification of 22.3% compared with the initial value. Wu et al. increased the coercivity from 14.6 kOe to 19.5 kOe and 24.0 kOe by Dy and Tb deposition, respectively [14]. The corresponding maximum energy products (BHmax) had values of 48.1 MGOe and 48.5 MGOe, respectively, representing slight decreases of 4.0% and 3.4%. The maximum overall magnetic performance value was Hcj (kOe) + (BH)max (MGOe) = 76.9.
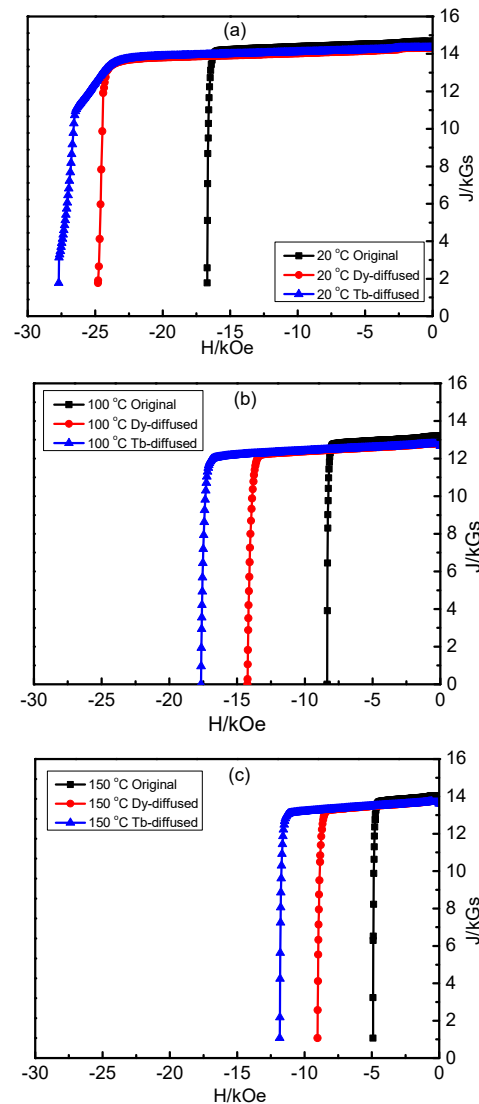

Figure 1. Demagnetization J–H curves of the magnets before and after Dy/Tb diffusion at 20 °C (**a**), 100 °C (**b**), and 150 °C (**c**).

Table 1. Magnetic properties and temperature coefficients at different temperatures of the magnets before and after Dy/Tb diffusion.

Sample	Temperature (°C)	Br (kGs)	α (%/°C)	Hcj (kOe)	β (%/°C)	(BH)max (MGOe)
Original	20	14.42		16.7		50.2
	100	13.18	−0.11	8.4	−0.62	41.5
	150	12.17	−0.12	4.9	−0.54	33
Dy-diffused	20	14.11		24.8		48.1
	100	12.80	−0.12	14.2	−0.53	39.3
	150	11.91	−0.12	9	−0.49	33.6
Tb-diffused	20	14.12		28.4		48.5
	100	12.78	−0.12	17.7	−0.47	39.3
	150	11.87	−0.12	11.8	−0.45	33.6

As shown in Figure 1 and Table 1, all of the magnets' magnetic properties decrease as temperature increases. Both the coercivity and remanence of magnets decrease with increasing temperatures, but the temperature sensibility of the coercivity is much larger than that of the remanence, which is consistent with previous reports [31,32]. The magnets after GBD with Dy/Tb possess much higher coercivity than that of the original magnet at 20 °C, 100 °C, and 150 °C, and the corresponding remanence as well as maximum magnetic energy product are slightly lower than those of the original magnet. Furthermore, the coercivity of the Tb-diffused magnet measured at 100 °C is higher than that of the original magnet measured at 20 °C, and both the Dy-diffused and Tb-diffused magnets show better coercivity at 150 °C than the original magnet measured at 100 °C. The higher temperature strengthens the thermal disturbance of the atomic magnetic moment of the magnet, which can lead to a reduction of magnetic properties. It can be inferred that Dy/Tb-diffused magnets display better resistance to thermal disturbances and higher coercivity than the original magnet at high temperatures. In addition, it can be observed that the Tb-diffused magnet possesses better magnetic properties than the Dy-diffused magnet at different temperatures (this will be discussed in Section 3.2).

As shown in Figure 1a, the J–H curve of the Tb-diffused magnet measured at 20 °C displays quite high coercivity compared with other curves, and it presents a special shoulder-like shape, indicating that not all grains can generate demagnetization domains under the same demagnetization field during the demagnetization process. That is to say, the demagnetization is not synchronized, and the grains with weaker demagnetization fields first form demagnetization domains. However, the grains with stronger demagnetization fields only form demagnetization domains under large demagnetization fields.

The corresponding demagnetization B–H curves in the second quadrant, as shown in Figure 2, reflect the maximum magnetic energy product of the magnets. The linear B–H curve is a very important characteristic that enables the magnets to be stable during operation. Under ideal conditions, it should be a straight line with a slope of 1. However, due to the low density, incomplete grain orientation, and non-magnetic phase formed in the process of magnet preparation, the curve shape deviates from the ideal state, and bending usually occurs when the residual magnetism approaches zero. The B–H curve of the original magnet measured at 20 °C shows a straight line, while the curves measured at 100 °C and 150 °C (Figure 2, line 4 and line 7) show an obvious knee-like feature. The Dy-diffused magnet retains linear B-H curves at 20 °C and 100 °C, and the knee-like feature occurs at 150 °C. However, the Tb-diffused magnet retains linear B–H curves even at 150 °C. This indicates that the microstructure and density of the magnets are improved after Dy/Tb diffusion. In particular, the microstructure of the Tb-diffused magnet is seen to approach the ideal state.
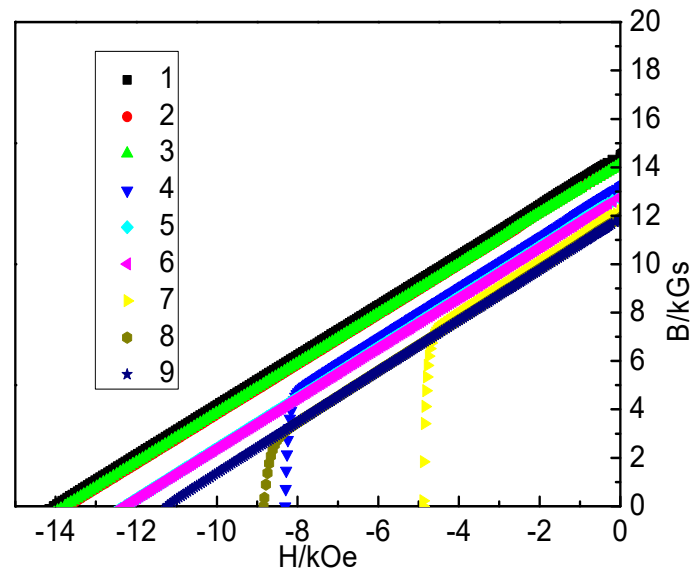
Figure 2. Demagnetization B–H curves of the magnets at different temperatures before and after Dy/Tb diffusion. 1–Original at 20 °C; 2–Dy-diffused at 20 °C; 3–Tb-diffused at 20 °C; 4–Original at 100 °C; 5–Dy-diffused at 100 °C; 6–Tb-diffused at 100 °C; 7–Original at 150 °C; 8–Dy-diffused at 150 °C; and 9–Tb-diffused at 150 °C.

Figure 3 shows the curves of remanence (a) and coercivity (b) of the magnets before and after GBD with Dy or Tb metals at 20–150 °C. The remanence temperature coefficient (α) and the coercivity temperature coefficient (β) of the magnets at 20–100 °C and 20–150 °C were calculated, and the results are listed in Table 2. The remanence temperature coefficients of the Dy- or Tb-diffused magnets both increase slightly from −0.11%/°C to −0.12%/°C at 20–100 °C, probably caused by non-magnetic phase formation in the process of GBD, while the coefficients of the three samples are almost the same at 20–150 °C, indicating that the high temperature is the main factor of thermal stability. Compared with the original magnet, the coercivity temperature coefficients of the Dy- or Tb-diffused magnets decrease significantly from −0.62%/°C to −0.53%/°C and −0.47%/°C, respectively, at 20–100 °C and from −0.54%/°C to −0.49%/°C and −0.45%/°C, respectively, at 20–150 °C, indicating better coercivity and thermal stability, which can be attributed to the optimized microstructure (this will be discussed in Section 3.2). In general, Dy- or Tb- diffused magnets exhibit better thermal stability than original magnets.
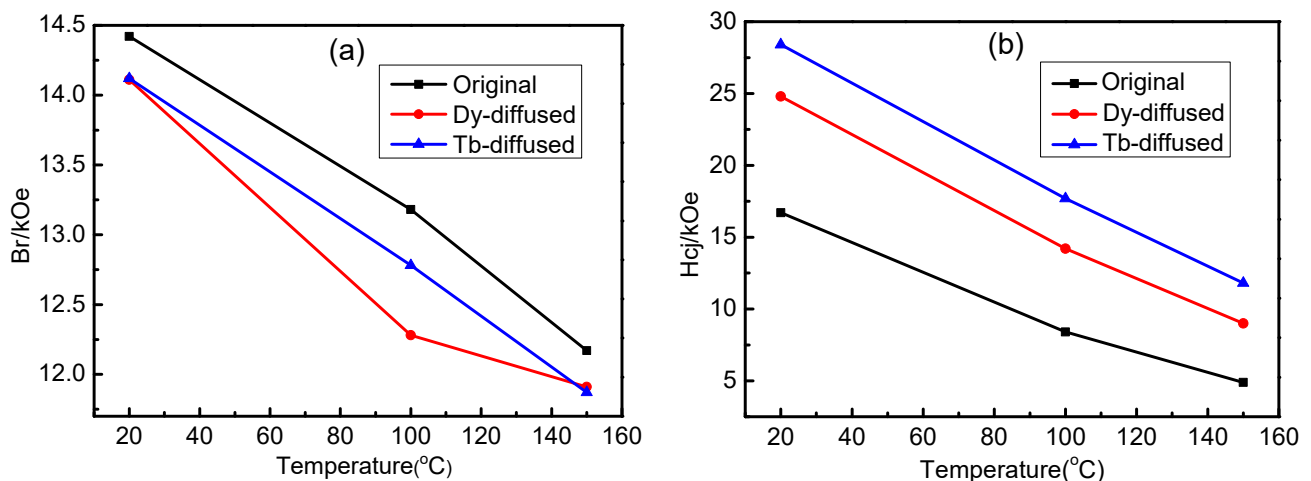

Figure 3. Remanence (**a**) and coercivity (**b**) of the magnets before and after GBD with Dy or Tb metals at 20–150 °C.

Table 2. Rare earth element (Nd, Pr, Dy, and Tb) content (wt%) of the magnets before and after Dy/Tb diffusion, measured by ICP.

Sample	Pr	Nd	Dy	Tb
Original	7.03	22.28	/	/
Dy-diffused	6.92	22.01	0.35	/
Tb-diffused	6.85	21.96	/	0.42

3.2. Microstructure and Chemical Composition

To comprehend the mechanism of coercivity enhancement, an EPMA test was performed to systematically study the microstructure and composition distribution in the vicinity of the surface of magnets, and the results are shown in Figure 4. As is known, bright contrast corresponds to phases containing more rare earth elements; the bright part along the GB in the original magnets shown in Figure 4a is the (Nd,Pr)-rich phase and the dark part is the $(Nd,Pr)_2Fe_{14}B$ grain phase. The corresponding elemental maps of Nd and Pr clearly indicate that most of the (Nd,Pr)-rich phases exist in the form of agglomerations at the corners of the $(Nd,Pr)_2Fe_{14}B$ main grains, while a small amount of (Nd,Pr)-rich phases exist in the form of a thin layer distributed along the GB and discontinuously surround the main grains. It can also be seen that there are some $(Nd,Pr)_2Fe_{14}B$ main grains that contact directly without a (Nd,Pr)-rich phase. The few discontinuous GB phases give rise to poor decoupling between the matrix grains, which corresponds well with the relatively low coercivity observed at 20 °C, as shown in Figure 1a and Table 1.

It can be seen from Figure 4b,c that after Dy or Tb diffusion, the bright agglomerations of Nd-Pr-rich phases become smaller and the bright GB phases become thicker compared with the original magnets shown in Figure 4a, and the distribution of the GB phases in the magnets becomes more uniform and continuous (Figure 4b,c). Furthermore, the GB phases in the Tb-diffused magnet are much more uniform and continuous compared to those in the Dy map and even cross-link with each other to form a network structure. From the mapping image of the Dy element (Figure 4b), it can be clearly observed that the enrichment of the Dy element mainly concentrates around the GB region, and similar results can be observed in the Tb map of the Tb-diffused magnet (Figure 4c), indicating that the Dy/Tb atoms penetrate into the magnet through GBD.

The eutectic reaction temperature of the $Nd-Nd_2Fe_{14}B$ system is 685 °C [33], which is much lower than the first heating treatment temperature (~900 °C) of GBD. The melting GB phases, including the Nd-Pr-rich phases, and the surface of the $(Nd,Pr)_2Fe_{14}B$ grains, can provide effective diffusion channels for HRE atoms. Furthermore, the added non-rare metals, including Al, Cu, Ga, etc., can form eutectic alloys with even lower melting points to provide wider diffusion channels for HRE atoms. Under the first heating treatment at 900 °C, Dy/Tb atoms diffuse into the magnets through the liquid GB phases. During the cooling process, the Nd and Pr atoms in the $(Nd,Pr)_2Fe_{14}B$ crystal lattice at the surface of the grains are partially replaced by mutual diffusion with Dy or Tb and enrich into the Nd-Pr-rich phases. The non-melting $(Nd,Pr)_2Fe_{14}B$ phase leads to the formation of a $(Nd,Pr)_2Fe_{14}B$ core, and the solidification of the Dy/Tb-rich liquid results in the formation of the $(Nd,Pr,Dy/Tb)_2Fe_{14}B$ shell, thus creating a core-shell structure, which can effectively increase magnetocrystalline anisotropy and prevent reverse magnetization domain nucleation. The resulting GB phases contain the increased Nd-Pr-rich phases and the $(Nd,Pr,Dy/Tb)_2Fe_{14}B$ shells, appearing much thicker as shown in Figure 4b,c, which can better wrap the $(Nd,Pr)_2Fe_{14}B$ grains and strengthen the demagnetization coupling effect. By subsequent optimal heat treatment at 520 °C, the distribution of the Nd-Pr-rich phase in the magnet becomes more uniform and continuous, reducing the exchange coupling of the $(Nd,Pr)_2Fe_{14}B$ grains still further. Since the non-melting grain phase is a solid phase and the diffusion rate of Dy/Tb in it is low, while the GB phase is a liquid phase and the diffusion of Dy/Tb in it is rapid, it can be inferred that the bulk diffusion of Dy/Tb can be ignored in this situation.
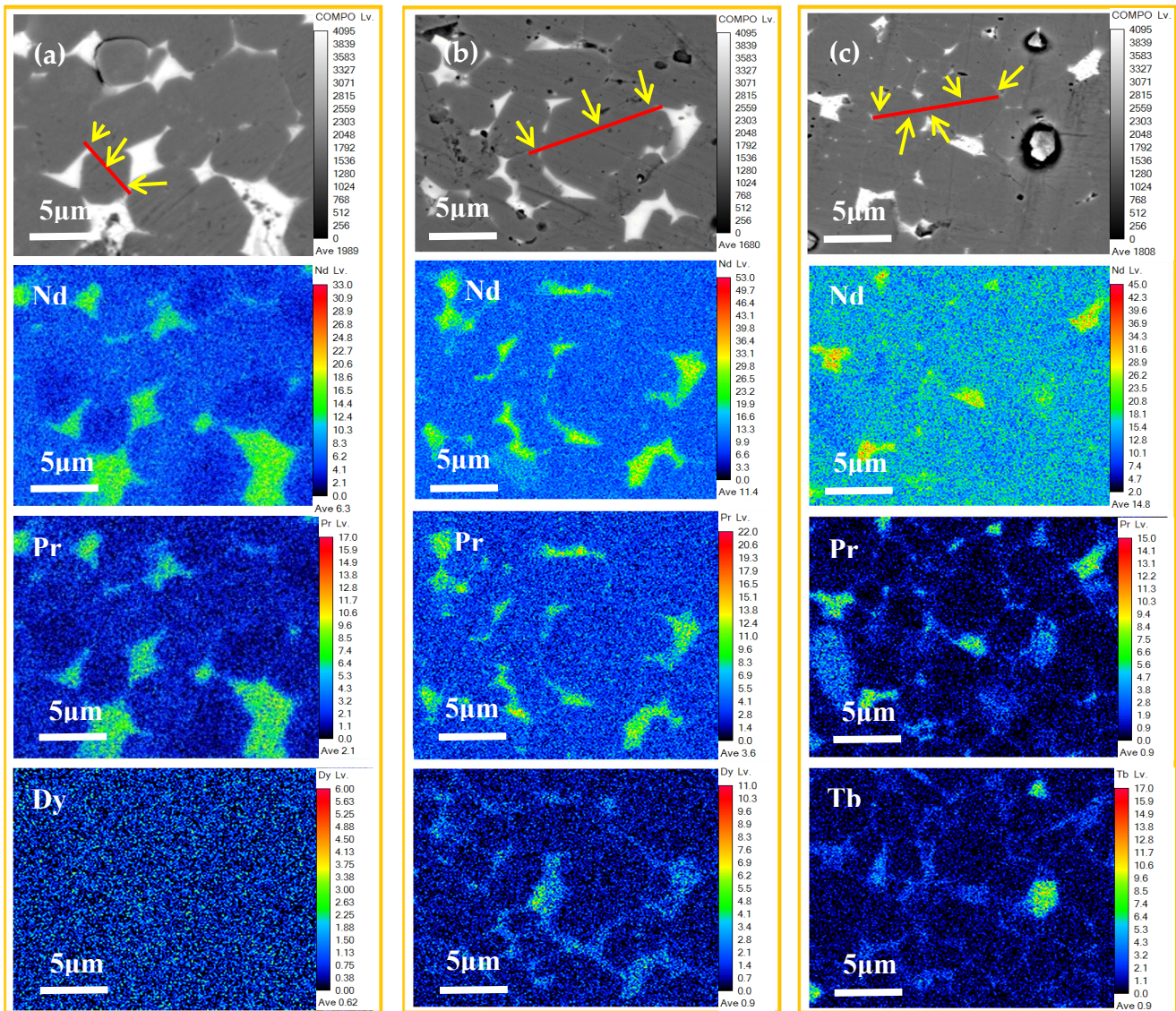
Figure 4. Back-scattered electron and EPMA element mapping images taken from the surface region of the original (**a**), Dy-diffused (**b**), and Tb-diffused (**c**) magnets (The red lines marked in the images are the line scan locations, yellow arrows are used to mark grain boundaries and grain interiors, as detailed in Figure 5).

Thus, it can be seen that the improvement in coercivity depends not only on the formation of $(Nd,Pr,Dy/Tb)_2Fe_{14}B$ shells in the surface region of the $(Nd,Pr)_2Fe_{14}B$ grains but also on the increased and optimized Nd-Pr-rich phases. In addition, the added non-rare metals (Al, Cu, Ga, etc.) also have positive effects on microstructure modification, such as wetting the GB phases and reducing defects at interfaces to suppress the nucleation of reverse domains, which is advantageous for the coercivity enhancement of magnets.

The corresponding distributions of rare earth elements (Nd, Pr, Dy, and Tb) determined by EPMA line scanning along the red line marked in Figure 4a–c are presented in Figure 5a–c, respectively. It can be observed that the light grey regions of the three samples corresponding to the bright GB phases all possess high Nd and Pr content. Moreover, after Dy or Tb GBD, the profiles display high Dy and Tb concentrations around the $(Nd,Pr)_2Fe_{14}B$ grains. In the non-grey regions, extremely low rare earth elements (Nd, Pr, Dy, and Tb) content is detected, which correspond to the $(Nd,Pr)_2Fe_{14}B$ grain cores. As a whole, the line scan profiles demonstrate that the concentration of Dy or Tb decreases

abruptly from the edge to the core of the grain, confirming that the Dy/Tb-rich shell is formed after diffusion. Otherwise, the interface would be diffuse instead of sharp.
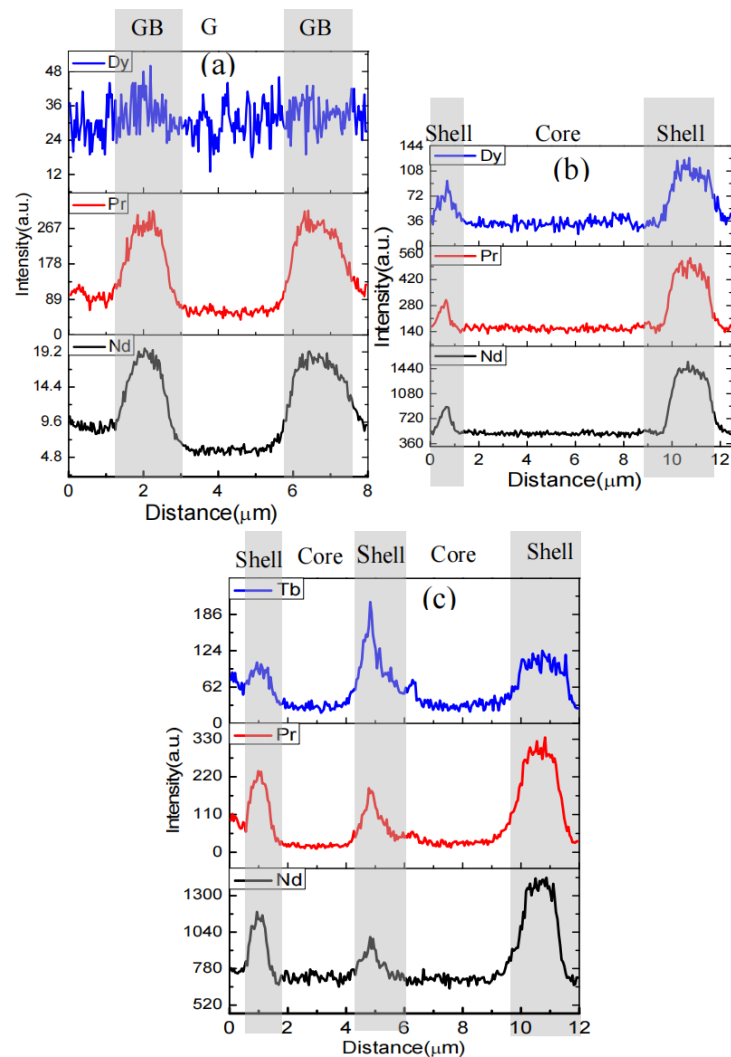

Figure 5. The corresponding line distribution of elements in (**a**) original, (**b**) Dy-diffused, and (**c**) Tb-diffused magnets from line scanning analysis along the red lines marked in Figure 4a–c, respectively. G: 2:14:1 grain; GB: grain boundary.

Since an optimized microstructure can result in coercivity enhancement, and higher coercivity at room temperature leads to better thermal stability [34,35], it can be inferred that Dy- or Tb-diffused magnets should exhibit better thermal stability than original magnets, which is consistent with the results observed in Section 3.1.

In addition, as discussed in Section 3.1, a Tb-diffused magnet possesses better magnetic properties at different temperatures than a Dy-diffused magnet. As shown in Figure 4b,c, after diffusion, the GB phases including Nd-Pr-rich layers and shells in the Tb-diffused magnet are much more uniform and continuous compared to those in the Dy map, and even cross-link with each other to form a network structure. This network structure can provide a much stronger reduction of the exchange coupling between the $(Nd,Pr)_2Fe_{14}B$ grains. The magnetocrystalline anisotropy of the Tb-rich shells is higher than that of the Dy-rich shells, suggesting stronger inhibition of the nucleation of reverse domains at low magnetic fields. Thus, the Tb-diffused magnet displays better coercivity.

Table 2 shows the average total Dy and Tb content in the Dy- and Tb-diffused magnets is 0.35 wt% and 0.42 wt%, respectively, when previously reported HREE-containing Nb-Fe-B magnets with comparable coercivity contain at least 2.4 wt% HREE [24,36], meaning

that around 80% of the Dy or Tb can be saved. Moreover, the total content of Nd and Pr in the magnets is reduced by 0.11 wt% and 0.17 wt%, respectively, through Dy substitution, while the content of Nb and Pr is reduced by 0.18 wt% and 0.32 wt%, respectively, through Tb substitution.

According to the experimental results, the Dy or Tb GBD in this work shows higher efficiency of HREE consumption, which can be mainly attributed to the formation of the special core-shell structure. In addition, and as mentioned above, the added non-rare metals (Al, Cu, Ga, etc.) may increase the quantity of the liquid phase, providing wider diffusion channels for the HREE atoms, thereby increasing the diffusion rate of the Dy or Tb. These metals also contribute to the coercivity enhancement of the magnets. In this case, we can achieve better coercivity using a lower amount of HREE. Low HREE content in magnets can reduce the adverse effects on remanence, which was why coercivity was greatly improved without or with only a slight decrease in remanence after diffusion, as discussed in Section 3.1. Therefore, this Dy or Tb element GBD process appears to be an effective way to increase coercivity with little HREE.

4. Conclusions

Dy- and Tb-diffused Nd-Fe-B magnets can be prepared by depositing Dy/Tb films on the surface using magnetron sputtering. The coercivity of the magnets is significantly enhanced by GBD, which can be attributed to the increased and optimized Nd-Pr-rich phases as well as the formation of $(Nd,Pr,Dy/Tb)_2Fe_{14}B$ shells around the $(Nd,Pr)_2Fe_{14}B$ grains. The consumption of Dy/Tb in this work is much lower than that of previously reported HREE-containing Nb-Fe-B magnets with comparable coercivity. In addition, the Dy- or Tb-diffused magnets also exhibit better thermal stability than the original magnets.

The excellent coercivity of Dy- or Tb-diffused magnets, combined with the high thermal stability of their magnetic properties, can open opportunities for potential high-temperature applications.

Author Contributions: Resources, X.-D.Z., M.W., Y.-J.Y., Q.W., F.W., P.-F.W., B.J., C.W. and B.Z.; writing—original draft preparation, M.W.; writing—review and editing, X.-D.Z. and Q.W. All authors have read and agreed to the published version of the manuscript.

Conflicts of Interest: The authors declare no conflict of interest.

References

1. Gutfleisch, O.; Willard, M.A.; Bruck, E.; Chen, C.H.; Sankar, S.G.; Liu, J.P. Magnetic materials and devices for the 21st century: Stronger, Lighter, and More Energy Efficient. *Adv. Mater.* **2011**, *23*, 821–842. [CrossRef] [PubMed]
2. Sugimoto, S. Current status and recent topics of rare-earth permanent magnets. *J. Phys. D Appl. Phys.* **2011**, *44*, 110–118. [CrossRef]
3. Deng, X.; Ge, J. Global wind power development leads to high demand for neodymium praseodymium (NdPr): A scenario analysis based on market and technology development from 2019 to 2040. *J. Clean. Prod.* **2020**, *277*, 123299. [CrossRef]
4. Gao, R.W.; Jiang, S.T.; Li, H.; Qiu, M.Y.; Guo, Y.C. A study on demagnetization process and coercivity mechanism in oriented sintered Nd-Fe-B permanent alloy. *Acta Phys. Sin.* **1989**, *38*, 439. (In Chinese)
5. Liu, X.B.; Altounian, Z. The partitioning of Dy and Tb in Nd-Fe-B magnets: A first-principles study. *J. Appl. Phys.* **2012**, *111*, 07A701. [CrossRef]
6. You, C.Y.; Zhu, J.; Tian, N.; Lu, Z.X. Coercivity enhancement of Nd-Fe-B thin film magnets through dy surface diffusion process. *J. Mater. Sci. Technol.* **2011**, *27*, 826–830. [CrossRef]
7. Hirosawa, S.; Yamaguchi, Y.; Tokuhara, K.; Yamamoto, H.; Fujimura, S.; Sagawa, M. Magnetic Properties of $Nd_2(Fe_{1-x}M_x)_{14}B$ Measured on Single Crystals (M = Al, Cr, Mn and Co). *IEEE Trans. Magn.* **1987**, *23*, 2120. [CrossRef]
8. Sepehri-Amin, H.; Une, Y.; Ohkubo, T.; Hono, K.; Sagawa, M. Microstructure of fine grained Nd-Fe-B sintered magnets with high coercivity. *Scr. Mater.* **2011**, *65*, 396. [CrossRef]
9. Boltich, E.B.; Oswald, E.; Huang, M.Q.; Hirosawa, S.; Wallace, W.E.; Burzo, E. Magnetic characteristics of R2Fe14B systems prepared with high purity rare earths (R = Ce, Pr, Dy, and Er). *J. Appl. Phys.* **1985**, *57*, 4106. [CrossRef]

10. Liu, W.; Li, Y.; Wu, D.; Yue, M.; Wang, Z.; Zha, S.; Liu, Y.; Yi, X.; Du, Y. Coercivity enhancement mechanism of grain boundary diffused Nd-Fe-B sintered magnets by magnetic domain evolution observation. *J. Rare Earths* **2021**, *39*, 682–688. [CrossRef]
11. Nakamura, H.; Hirota, K.; Shimao, M. Magnetic properties of extremely small Nd-Fe-B sintered magnets. *IEEE Trans. Magn.* **2005**, *41*, 3844–3846. [CrossRef]
12. Chen, W.; Luo, J.M.; Guan, Y.W.; Huang, Y.L.; Chen, M.; Hou, Y.H. Grain boundary diffusion of Dy films prepared by magnetron sputtering for sintered Nd-Fe-B magnets. *J. Phys. D Appl. Phys.* **2018**, *51*, 185001. [CrossRef]
13. Suzuki, H.; Satsu, Y.; Komuro, M. Magnetic properties of a Nd-Fe-B sintered magnet with Dy segregation. *J. Appl. Phys.* **2009**, *105*, 07A734. [CrossRef]
14. Wu, B.; Zhang, Q.; Li, W.; Ding, X.; Yang, L.; Ghafar Wattoo, A.; Zhang, L.; Mao, S.; Song, Z. Grain boundary diffusion of magnetron sputter coated heavy rare earth elements in sintered Nd-Fe-B magnet. *J. Appl. Phys.* **2018**, *123*, 245112. [CrossRef]
15. Bae, K.H.; Lee, S.R.; Kim, H.J.; Lee, M.W.; Jang, T.S. Effect of oxygen content of Nd–Fe–B sintered magnet on grain boundary diffusion process of DyH2 dip-coating. *J. Appl. Phys.* **2015**, *118*, 203902. [CrossRef]
16. Guo, S.; Zhang, X.F.; Ding, G.F.; Chen, R.J.; Lee, D.; Yan, A. Coercivity enhancement of sintered Nd-Fe-B magnets by chemical bath deposition of TbCl₃. *J. Appl. Phys.* **2014**, *115*, 17A754. [CrossRef]
17. Hirota, K.; Nakamura, H.; Minowa, T.; Honshima, M. Coercivity enhancement by the grain boundary diffusion process to Nd-Fe-B sintered magnets. *IEEE Trans. Magn.* **2006**, *42*, 2909. [CrossRef]
18. Hu, S.Q.; Peng, K.; Chen, H. Influence of annealing temperature on the Dy diffusion process in NdFeB magnets. *J. Magn. Magn. Mater.* **2017**, *426*, 340. [CrossRef]
19. Li, D.; Suzuki, S.; Kawasaki, T.; Machida, K. Grain Interface Modification and Magnetic Properties of Nd-Fe-B Sintered Magnets. *Jpn. J. Appl. Phys.* **2008**, *47*, 7876. [CrossRef]
20. Sepehri-Amin, H.; Ohkubo, T.; Hono, K. Grain boundary structure and chemistry of Dy-diffusion processed Nd-Fe-B sintered magnets. *J. Appl. Phys.* **2010**, *107*, 09A745. [CrossRef]
21. Loewe, K.; Benke, B.; Kubel, C.; Lienig, T.; Skokov, K.P.; Gutfleisch, O. Grain boundary diffusion of different rare earth elements in Nd-Fe-B sintered magnets by experiment and FEM simulation. *Acta Mater.* **2017**, *124*, 421. [CrossRef]
22. Lu, K.C.; Bao, X.Q.; Tang, M.H.; Chen, G.X.; Mu, X.; Li, J.H.; Gao, X.X. Boundary optimization and coercivity enhancement of high (BH)max Nd-Fe-B magnet by diffusing Pr-Tb-Cu-Al alloys. *Scr. Mater.* **2017**, *138*, 83. [CrossRef]
23. Popov, A.G.; Vasilenko, D.Y.; Puzanova, T.Z.; Shitov, A.V.; Vlasyuga, A.V. Effect of diffusion annealing on the hysteretic properties of sintered Nd-Fe-B magnets. *Phys. Met. Metallogr.* **2011**, *111*, 471. [CrossRef]
24. Sepehri-Amin, H.; Ohkubo, T.; Hono, K. The mechanism of coercivity enhancement by the grain boundary diffusion process of Nd-Fe-B sintered magnets. *Acta Mater.* **2013**, *61*, 1982. [CrossRef]
25. Cao, X.J.; Chen, L.; Guo, S.; Fan, F.C.; Chen, R.J.; Yan, A. Effect of rare earth content on TbF3 diffusion in sintered Nd-Fe-B magnets by electrophoretic deposition. *Scr. Mater.* **2017**, *131*, 24. [CrossRef]
26. Cao, X.J.; Chen, L.; Guo, S.; Li, X.B.; Yi, P.P.; Yan, A.R.; Yan, G.L. Coercivity enhancement of sintered Nd-Fe-B magnets by efficiently diffusing DyF3 based on electrophoretic deposition. *J. Alloys Compd.* **2015**, *631*, 315. [CrossRef]
27. Komuro, M.; Satsu, Y.; Suzuki, H. Increase of coercivity and composition distribution in fluoride-diffused NdFeB sintered magnets treated by fluoride solutions. *IEEE Trans. Magn.* **2010**, *46*, 3831. [CrossRef]
28. Loewe, K.; Brombacher, C.; Katter, M.; Gutfleisch, O. Temperature-dependent Dy diffusion processes in Nd-Fe-B permanent magnets. *Acta Mater.* **2015**, *83*, 248. [CrossRef]
29. Xie, H.Z. *Theory and Practice of NdFeB Oxygen Free Process Technology*; Metallurgical Industry Press: Beijing, China, 2018; pp. 1–5.
30. Li, Z.Q.; Zhang, Y.M.; Zhao, N.; Liu, L.; Mao, C.Y. A Manufacturing Method of Neodymium Iron Boron with High Coercivity. China Patent CN105655077B; (Application granted 17 October 2017),
31. Chen, F.; Zhang, L.; Jin, Y.; Cheng, Y. Simultaneous enhancement of the coercivity and remanence at high temperatures in a sintered Nd-Fe-B magnet after grain boundary diffusion with Dy60Co40 alloy. *Mater. Charact.* **2018**, *144*, 547. [CrossRef]
32. Chen, F.G. Recent progress of grain boundary diffusion process of Nd-Fe-B magnets. *J. Magn. Magn. Mater.* **2020**, *514*, 167227. [CrossRef]
33. Seelam, U.M.R.; Ohkubo, T.; Abe, T.; Hirosawa, S.; Hono, K. Faceted shell structure in grain boundary diffusion-processed sintered Nd-Fe-B magnets. *J. Alloys Compd.* **2014**, *617*, 884. [CrossRef]
34. Xu, J.Y.; Hu, C.L.; Zhang, J.T.; Dong, S.Z.; Chen, H.S. Research progress of high temperatures stable sintered Nd-Fe-B magnets. *Met. Funct. Mater.* **2022**, *29*, 106.
35. Hu, X.J.; Guo, Z.H.; Pan, W.; Li, W. The effects of intrinsic coercivity Hcj on the thermal stability of Nd-Fe-B magnets. *Met. Funct. Mater.* **2004**, *1*, 2.
36. Wei, G.; Zhao, M.; Xia, X.; Ju, J.; Du, Y.; Huang, Y.; Tang, X.; Yin, W.; Chen, R.; Yan, A. Ultrahigh coercivity and excellent thermal stability of hot-deformed Nd-Fe-B magnets by the diffusion of (Pr, Nd)-Dy-Cu-Al. *J. Alloys Compd.* **2023**, *960*, 170756. [CrossRef]